Controllable Non-Markovianity for a Spin Qubit in Diamond

J. F. Haase,[1,*] P. J. Vetter,[2] T. Unden,[2] A. Smirne,[1] J. Rosskopf,[1] B. Naydenov,[2] A. Stacey,[3,4] F. Jelezko,[2] M. B. Plenio,[1] and S. F. Huelga[1]

[1]*Institut für Theoretische Physik und IQST, Albert-Einstein-Allee 11, Universität Ulm, D-89069 Ulm, Germany*
[2]*Institut für Quantenoptik und IQST, Albert-Einstein-Allee 11, Universität Ulm, D-89069 Ulm, Germany*
[3]*Element Six, Harwell Campus, Fermi Avenue, Didcot OX11 0QR, United Kingdom*
[4]*Centre for Quantum Computation and Communication Technology, School of Physics, University of Melbourne, Parkville, Melbourne, Victoria 3010, Australia*

(Received 5 March 2018; published 9 August 2018)

We present a flexible scheme to realize non-Markovian dynamics of an electronic spin qubit, using a nitrogen-vacancy center in diamond where the inherent nitrogen spin serves as a regulator of the dynamics. By changing the population of the nitrogen spin, we show that we can smoothly tune the non-Markovianity of the electron spin's dynamics. Furthermore, we examine the decoherence dynamics induced by the spin bath to exclude other sources of non-Markovianity. The amount of collected measurement data is kept at a minimum by employing Bayesian data analysis. This allows for a precise quantification of the parameters involved in the description of the dynamics and a prediction of so far unobserved data points.

DOI: 10.1103/PhysRevLett.121.060401

Introduction.—Realistic physical systems are subject to environmental noise which affects their quantum dynamics [1–4]. The rapidly advancing development of quantum technologies which are aiming to make use of quantum dynamics in a broad range of applications such as quantum computing [5], quantum cryptography [6], quantum simulation [7], quantum sensing [8], and quantum metrology [9] calls for a detailed understanding of these noise sources that may alter their function.

Typically, environmental noise does not induce featureless white noise on the system, but it can exhibit spatial and temporal correlations that can be used when addressing the system-environment interaction. Non-Markovian noise, which is the subject of this Letter, exhibits a temporal correlation originating from some slow internal evolution of the environment [2,10–12]. On the one hand, one may combat such non-Markovian noise by means of dynamical decoupling methods, which allows us to partially shield the system of interest from the impact of noise [13–15]. On the other hand, it has been recognized early on that noise may also be a resource, e.g., for the generation of entangled states [16,17]. In particular, one may explore the specific advantages that colored noise can provide here; this has been shown in several reports [16,18–25]. More recently, the introduction of definite and general ways to quantify the degree of non-Markovianity of quantum dynamics [10,11,26–31] has provided a further boost for the quantitative understanding of the role of non-Markovianity in different settings and has increased the ability to manipulate open-system dynamics, in view of possible strategies to reduce the detrimental effects of noise. In fact, an extended control over the amount of non-Markovianity has been demonstrated experimentally in trapped ion systems [32] and photonic setups [33–36].

Here, we want to take a further step in the direction of the full control of the non-Markovianity of quantum dynamics by investigating theoretically and experimentally the different dynamical regimes experienced by an electronic spin qubit of a nitrogen-vacancy (N-V) center in diamond [37,38]. We stress that the system at hand is undergoing a genuine open-system evolution, in which the main source of noise inducing non-Markovianity, namely, the nitrogen nuclear spin, is an inherent part of the N-V center. The procedure in our work consists of two steps: first a characterization of the natural background noise to exclude any source of non-Markovianity besides the nitrogen spin. Therefore, we examine the free-induction decay (FID) of the electron spin while the interaction with the nitrogen spin is suppressed. The FID is induced by various sources, such as ^{13}C spins or additional nitrogen impurities, the diamond surface, but also experimental limitations, e.g., drifts in the optical setup. We show that the obtained data can be analyzed efficiently using Bayesian inference methods [39–42]. These allow for a large number of free parameters and determine from a multidimensional probability distribution the most likely parameter set describing the data. They are therefore particularly well suited to fully characterize the open-system dynamics at hand. Second, we study how to use the nitrogen spin inherent to the N-V center to control the degree of non-Markovianity of the electronic spin. Therefore, we manipulate the polarization of the nitrogen spin to induce collapses and revivals on the electronic spin coherence, while the polarization direction of the nitrogen spin defines the amplitude of these collapses

and revivals. The degree of non-Markovianity corresponding to the different configurations is measured and compared with the theoretical predictions provided by the Bayesian data analysis, showing that we can achieve full control on the amount of non-Markovianity involved in the evolution of this solid-state system.

Model.—The N-V center is a point defect in the diamond lattice consisting of a substitutional nitrogen atom adjacent to a vacancy. Its negatively charged state possesses an electronic spin triplet ^{3}A ground state [37] with a zero field splitting of $\Delta = 2\pi \cdot 2.87$ GHz between the $|m_s = 0\rangle$ and $|m_s = \pm 1\rangle$ states (from now on we denote $S_z|m_s = i\rangle = i|m_s = i\rangle = i|i\rangle$). Interaction with the inherent nitrogen nuclear spin results in a hyperfine splitting of the $|\pm 1\rangle$ states, depending on the nitrogen isotope, here ^{14}N ($I = 1$), which results in a hyperfine splitting of $A_\parallel \approx 2.14$ MHz [45]. We use a low nitrogen (< 1 ppb) diamond with a concentration of 0.2% ^{13}C nuclear spins to prolong the electron spin coherence time. We identified a native N-V center, located deep (a few μm) below the diamond surface. The Hamiltonian of this configuration is given by [38]

$$H_{\text{lab}} = \Delta S_z^2 + \gamma_e B_z S_z + P I_z^2 + \gamma_N B_z I_z + S_z A_\parallel I_z + A_\perp (S_x I_x + S_y I_y) + H_R \quad (1)$$

where $S(I)$ are the electron (^{14}N) spin-1 operators, B_z is a magnetic field applied along the N-V center symmetry axis, and the electronic (^{14}N) gyromagnetic ratio is labeled by γ_e (γ_N), the quadrupole splitting P and orthogonal interaction $A_\perp$. An applied field of $B_z = 453$ G lifts the degeneracy between the $|\pm 1\rangle$ states. The Hamiltonian H_R contains all the remaining terms originating from the environment of the N-V center, e.g., ^{13}C spins and other nitrogen impurities, including their coupling to the electron spin, but may also be considered as an effective Hamiltonian responsible for experimental imperfections [43,44]. We apply the secular approximation due to the large zero field splitting $\Delta \gg A_\perp \approx 2\pi \cdot 2.70$ MHz [45], which prohibits flips of the ^{14}N spin and also removes all terms in H_R not coupling to S_z [43]. Because all free energy terms commute with the remaining interaction Hamiltonian $S_z A_\parallel I_z$, these terms can be removed in a rotating frame yielding

$$H = S_z A_\parallel I_z + H_R. \quad (2)$$

We employ the electron spin as a noise sensor for the environment choosing the subspace spanned by the $|0\rangle$ and $|-1\rangle$ state as an artificial qubit. Because of the pure dephasing Hamiltonian, the reduced density matrix of the electron spin only experiences a modulation of the coherence elements; hence, the FID is efficiently measured by a Ramsey experiment, whose scheme is sketched in Fig. 1(a). The electron spin preparation and readout is achieved optically. The spin-selective, nonradiative intersystem crossing to a metastable singlet state between the electronic excited and ground state [37] enables a strong electron spin polarization into the $|0\rangle$ ground state. The higher photoluminescence intensity of the $|0\rangle$ state allows us to determine the electron spin state. We polarize the nitrogen nuclear spin in the $|m_I = 1\rangle$ state by optical pumping [46] and rotate it by a radio-frequency pulse $R(\phi)$ to a desired coherent state. After polarization, a $\pi/2$ pulse flips the electron spin to the superposition state $|\psi\rangle = (|0\rangle + |-1\rangle)/\sqrt{2}$. For a time t the system will evolve freely depending on the electron spin state as depicted in Fig. 1(b), i.e., according to the conditional Hamiltonian $H_i = \langle i|H|i\rangle$. Assuming an initial product state $\rho = \rho^{(e)} \otimes \rho^{(N)} \otimes \rho^{(R)}$ [with $\rho^{(e)} = |\psi\rangle\langle\psi|$ and $\rho^{(R)}$ arbitrary], the dynamic of the electron spin is completely described by the coherence modulation, i.e.,

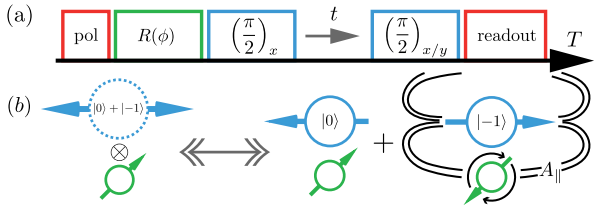

FIG. 1. The sequence for the Ramsey experiments in (a) consists of a preparation phase, where the pulse $R(\phi)$ can control the population of the ^{14}N spin, two $\pi/2$ pulses (either x or y phase) on the electron spin, and the subsequent readout. During the free period t, the spins undergo the conditional evolution illustrated in (b). If the electron spin populates $|-1\rangle$, it produces a hyperfine field which induces rotations of the ^{14}N spin. Therefore, the pair switches continuously between a product (left) and an entangled state (right) [the roles of ^{14}N and the electron spin are interchangeable].

$$\rho^{(e)}_{0,-1}(t) = \langle 0|\text{tr}_{N,R}[\rho(t)]|-1\rangle \propto \text{tr}_{N,R}[e^{-itH_0}\rho^{(N)} \otimes \rho^{(R)} e^{itH_{-1}}], \quad (3)$$

where $\text{tr}_{N,R}[\bullet]$ denotes the partial trace over the nitrogen and bath degrees of freedom. Assuming no residual population left in $|-1\rangle$, the length of the Bloch vector associated with the qubit in the $\{|0\rangle, |1\rangle\}$ subspace is equivalent to the coherence. This length can directly be calculated as

$$r(t) = [p_0^2 + p_1^2 + p_{-1}^2 + 2p_0(p_1 + p_{-1})\cos(A_\parallel t) + 2p_1 p_{-1}\cos(2A_\parallel t)]^{1/2}|L(t)|, \quad (4)$$

where $L(t) = \text{tr}[e^{-it\langle 0|H_R|0\rangle}\rho^{(R)} e^{it\langle -1|H_R|-1\rangle}]$ and p_i is the initial population in the state $|m_I = i\rangle$ of the nitrogen spin. Using the normalization constraint, we parametrize $p_1 = p\cos^2(\phi/2)$, $p_0 = p\sin^2(\phi/2)$, and $p_{-1} = 1 - p$, where ϕ is a mixing angle and p is the amount of population in the desired subspace of $|m_I = 0, 1\rangle$. For the readout, the electron spin is rotated back to the z axis (either around

x or y), and after a subsequent readout pulse the fluorescence light is recorded proportional to $r(t)$. The detailed calculation of $L(t)$ quickly becomes tedious, as it requires explicit knowledge about the bath and the related coupling strengths. However, it can often be modeled effectively as $L(t) = \exp[-(t/T_2^*)^2]$ [47].

Since we are dealing with a pure dephasing dynamics, all common definitions of (non-)Markovianity coincide [48]. Explicitly, the dynamics is non-Markovian if and only if $dr(t)/dt > 0$ for some time $t \geq 0$. On the other hand, the different ways to quantify the degree of non-Markovianity are not equivalent [49,50]. In particular, we choose to measure the amount of non-Markovianity via the trace distance [27], which identifies non-Markovian evolutions as those with a backflow of information from the environment. By taking an integral over all the time intervals where the trace distance increases and maximizing over the couple of initial states, one can then define a measure of non-Markovianity $\mathcal{N}$. For the model at hand, this is simply given by

$$\mathcal{N} = \sum_m r(\tau'_m) - r(\tau_m), \tag{5}$$

where m labels all intervals (τ_m, τ'_m) with $r(\tau'_m) - r(\tau_m) > 0$. Indeed, we have $\mathcal{N} = 0$ for a Markovian evolution, corresponding to a monotonic decay of the electronic coherence, while any revival in the coherence will induce an increase of the non-Markovianity.

In order to analyze the collected data and predict unperformed measurements, we set up a probabilistic model (see also the Supplemental Material [51]). Given a prior (probability) distribution $\mathcal{P}(\Theta)$ on a set Θ of parameters to be estimated, Bayes' theorem provides the posterior distribution $\mathcal{P}(\Theta|\mathcal{X})$ quantifying the probability that the model employing Θ accurately describes the data $\mathcal{X}$, $\mathcal{P}(\Theta|\mathcal{X}) \propto \mathcal{P}(\mathcal{X}|\Theta)\mathcal{P}(\Theta)$. Here $\mathcal{P}(\mathcal{X}|\Theta)$ is the likelihood that we obtain $\mathcal{X}$ given Θ. A Markov Chain Monte Carlo algorithm samples the posterior distribution after specifying the likelihood and prior yielding two main advantages: First, any correlation between different parameters is inherent to the model, and, second, error bounds arise as a natural result from the sampling process. Using probability theory, marginals for all elements in Θ can be obtained [40,41].

FID decay under the influence of the bath.—In a preliminary experiment we explore the agreement of the FID envelope induced by H_R with a monotonic decay to exclude contributions to a non-Markovian evolution. Therefore, polarization of the ^{14}N spin is performed such that $p_0 = 1$ [and $R(\phi) \equiv \mathbb{1}$]. This enables a measurement of $|L(t)|$. Figure 2(a) shows the FID envelope. We model the observed likelihood distribution by a normal distribution with a mean $\mu = r(t) + d$ and $|L(t)| = \exp(-\sum_{i=0}^{5} a_i t^i)$; see also Eq. (4). Here, a_0 is a constant to normalize the measured contrast and d is a possible bias in the asymptotic regime. After 50 000 iterations of the chosen sampling algorithm [51], we plot the red curve using the medians of the sampled parameters and the marginals of the posterior distribution for all $a_{i>0}$ in the insets. The experimentally measured contrast at specific times is shown with black dots. The FID envelope is well characterized by an $L(t) = \exp[-(t/T_2^*)^2]$; i.e., the dynamic is fully Markovian. We extract the characteristic timescale from the marginal of a_2 (we take the median as the point estimate and denote it by $\bar{\bullet}$) and obtain $T_2^* = 22.262$ μs, where the 95% highest posterior density (HPD) interval (i.e., 95% of the sampling values lie in that region) is $[21.878, 22.868]$ μs. Coherence envelopes of this form are extremely useful for frequency estimation using entangled states, since the Gaussian decay ensures a superclassical scaling of the estimation error with the number of probes [22].

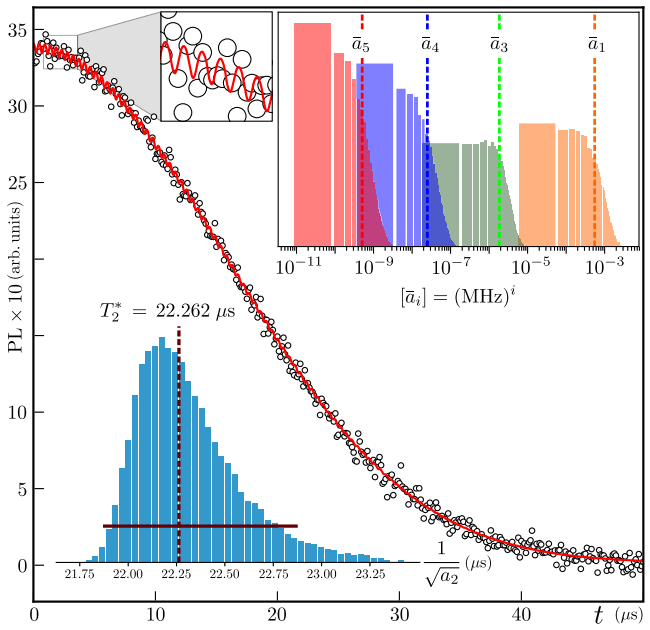

FIG. 2. The FID curve of the N-V center in units of the measured photoluminescence (PL). The negligible values of the decay constants $\bar{a}_i$ in the top right histogram of sampled values supports the purely Gaussian shape of $L(t)$. The histogram in the lower left assembles the distribution for T_2^* with the HPD interval marked by the horizontal line. From the initial oscillations at short times, the Bayesian method can extract also other parameters (the distributions are not shown), as $p = 0.972$ with HPD [0.943, 1], $\phi = 0.191$ with HPD [0.151, 0.227], and $A_\parallel = 2\pi \times 2.143$ MHz, where HPD $2\pi \times [2.137, 2.148]$ MHz.

A careful examination of the short time regime reveals oscillations in the FID curve (see the inset in Fig. 2), suggesting that the nitrogen spin is not fully polarized, as confirmed by the Bayesian method exploiting Eq. (4) of our model [51]. The procedure is able to extract the different contributions to the decay stemming from the bath $[L(t)]$, but also the parameters describing the ^{14}N spin; i.e., we obtain the coupling strength $A_\parallel$ and the parameters ϕ, p (for

the values, see Fig. 2) for the population distribution [up to the symmetry in $|m_I = \pm 1\rangle$, which is not resolvable in such an experiment; see Eq. (4)].

Tunable non-Markovianity.—An imperfectly polarized ^{14}N spin, i.e., a coherent or incoherent mixture of I_z eigenstates, induces oscillations on the electron spin coherence (see Fig. 2); consequently, the reduced electron spin state undergoes a non-Markovian evolution. Vice versa, any population of the ^{14}N spin state undergoes the conditional evolution governed by the Hamiltonian, Eq. (2). At the point of maximal achievable correlations [Fig. 1(b), right], the reduced state of the electron spin has reached its point of minimal coherence. Following is an increase in coherence corresponding to a reduction of correlations [55] between the two spins. Consequently, changing the orientation of the polarization of the nitrogen spin allows us to control the non-Markovianity of the electron spin in a continuous manner.

In order to measure experimentally the amount of non-Markovianity, we follow again the Ramsey scheme, Fig. 1(a). After polarization, the nitrogen spin population can be manipulated by a resonant radio-frequency pulse $R(\phi)$ to create the nuclear spin state $|\psi_I\rangle = \sin(\phi/2)|m_I = 0\rangle + \cos(\phi/2)|m_I = 1\rangle$. We track the evolution of the electron spin for 14 different values of ϕ up to a maximum time of $T = 1.226\ \mu$s and record the oscillations in the coherence.

Let us now describe the probabilistic model for this specific setup (see [51] for further details). First, note that a theoretical measure of non-Markovianity as defined in Eq. (5) requires processed data (e.g., fits). Otherwise, fluctuations will dominate the measure; e.g., for a constant coherence function fluctuations of the measurement results accumulate and give a positive measure. To avoid this issue we exploit the oscillatory nature of the modulation and stop the recording of the oscillation before finishing an integer number of periods. The requirement of an increase of the coherence in Eq. 3 is then relaxed, and the sum runs over all intervals, so that the fluctuations in the data are averaged out. The model for the measure then possesses the simple form $\mathcal{N}'(\phi) = C(\phi)\{r[\phi, p(\phi), T] - 1\}$, where $C(\phi)$ is a parameter describing the measurement contrast [56] and $1 - p(\phi)$ is the population left in $|m_I = -1\rangle$. We infer the model on the measured data to obtain the information of these functional dependencies; see the upper part of Fig. 3. Afterwards, the obtained posterior distribution is used to predict $\mathcal{N}'(\phi)$ for different values of ϕ by drawing multiple samples and calculating the mean values.

The theoretical and experimental results are reported in Fig. 3. In the lower part, black dots mark $\mathcal{N}'(\phi)$ for the 14 measured instances of ϕ. The theory curve according to Eq. (5) in black (dotted) is rescaled to match the values of the contrast. Its deviation from the red curve, which illustrates the expectation value of $\mathcal{N}'(\phi)$ sampled with respect to the posterior distribution, is due to the fact that

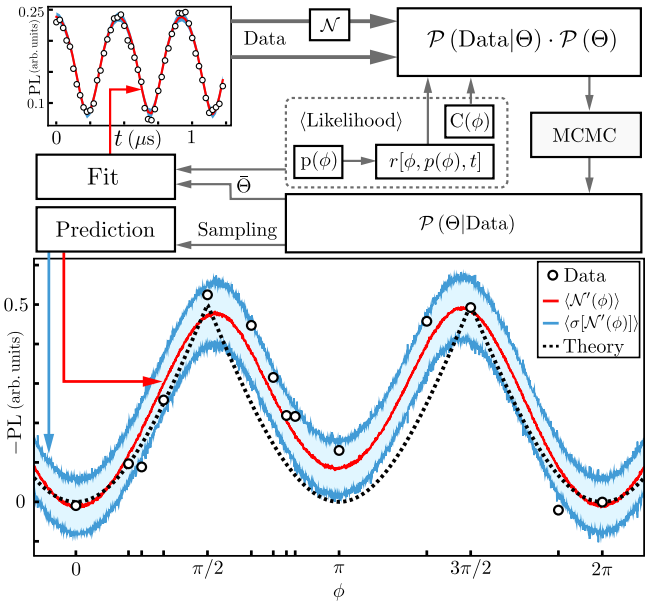

FIG. 3. Ramsey measurements are performed for different values of ϕ (top left, only $\phi = 2\pi/3$ is shown, black circles), and the non-Markovianity measure $\mathcal{N}'$ (lower plot, black circles) is evaluated, which are both fed as observations into the likelihood distribution. The expectation value of the likelihood is constructed according to $\mathcal{N}'$, while the prior distributions are taken as normal distributions around physically reasonable values [51]. The HPD parameter set $\bar{\Theta}$ can be plugged into the model defining the likelihood, which results in the maximum *a posteriori* inference (red curve) to the Ramsey data. The posterior distribution is sampled for different and, crucially, not measured values of ϕ. This results in an expectation value $\langle\mathcal{N}'\rangle$ which is taken with respect to the posterior, shown as the red curve in the lower plot along with the blue region marking the standard deviation. The black dotted line corresponds to the theory result neglecting the varying readout contrast and the remaining population in $|m_I = -1\rangle$.

the Bayesian model includes the angle dependent contrast and the nitrogen population left in $|m_I = -1\rangle$. In other words, the posterior distribution predictions of our parameters, together with the model in Eq. (4) enable us to simulate further measurements of the experiment. We show the standard deviation of the sampling as the blue region, which covers most of the actual measurements. This standard deviation is due to error sources not included explicitly in the model, e.g., the remaining population of the electron spin in $|m_s = 1\rangle$ or drifts in the experimental setup.

Conclusion.—We experimentally demonstrate the control of the degree of non-Markovianity in the dynamics of an N-V center electron spin. To that end, we first examine the FID envelope and employ a Bayesian probabilistic model to ensure that the degree of non-Markovianity is induced by the residual background resulting mainly from a nuclear spin environment. Subsequently, we exploit the inherent ^{14}N spin to induce modulations on the electron spin

coherence. The ^{14}N provides us with a natural source of non-Markovianity, which, depending on its initial preparation, will be able to exchange a certain amount of information with the electron spin, influencing the evolution of the latter. Despite the initial control, the ^{14}N remains a natural source of non-Markovianity as no further interventions after the preparation have to be performed. The experimental effort is kept sufficiently low by using Bayesian techniques, which allow us to predict the shape of the considered non-Markovianity measure. Let us also mention that the scheme presented may be extended by the utilization of strongly coupled ^{13}C spins or interacting N-V centers. Using the same technique as described here, additional parameters to shape the evolution can be introduced. Further modifications could be implemented as well via a classical driving with a random, but temporally correlated, amplitude.

In summary, the configuration investigated here allows the assembly of an experimental platform with intrinsic non-Markovianity. This provides a building block for the systematic investigation of memory effects in the performance of, e.g., quantum sensors and quantum metrology protocols, as well as facilitating the controllable inclusion of memory in quantum simulations of open quantum system dynamics.

This work was supported by the ERC Synergy grant BioQ, the EU project QUCHIP, the DFG, BMBF, and the Volkswagenstiftung. We acknowledge discussions with the team of Jiangfeng Du. We thank Matthew Markham for the sample preparation.

Note added.—Recently, related experimental results on non-Markovian features of N-V center dynamics were reported in [57,58].

*Corresponding author.
haasejanf@gmail.com

[1] H. Carmichael, *An Open Systems Approach to Quantum Optics* (Springer-Verlag, Berlin, 1993).
[2] H.-P. Breuer and F. Petruccione, *The Theory of Open Quantum Systems* (Oxford University Press, New York, 2002).
[3] C. W. Gardiner and P. Zoller, *Quantum Noise: A Handbook of Markovian and Non-Markovian Quantum Stochastic Methods with Applications to Quantum Optics* (Springer, Berlin, 2004).
[4] Á. Rivas and S. F. Huelga, *Open Quantum Systems* (Springer, New York, 2012).
[5] M. A. Nielsen and I. L. Chuang, *Quantum Computation and Quantum Information* (Cambridge University Press, New York, 2000).
[6] N. Gisin, G. Ribordy, W. Tittel, and H. Zbinden, Rev. Mod. Phys. **74**, 145 (2002).
[7] I. M. Georgescu, S. Ashhab, and F. Nori, Rev. Mod. Phys. **86**, 153 (2014).
[8] C. L. Degen, F. Reinhard, and P. Cappellaro, Rev. Mod. Phys. **89**, 035002 (2017).
[9] V. Giovannetti, S. Lloyd, and L. Maccone, Science **306**, 1330 (2004).
[10] Á. Rivas, S. F. Huelga, and M. B. Plenio, Rep. Prog. Phys. **77**, 094001 (2014).
[11] H.-P. Breuer, E. M. Laine, J. Piilo, and B. Vacchini, Rev. Mod. Phys. **88**, 021002 (2016).
[12] I. de Vega and D. Alonso, Rev. Mod. Phys. **89**, 015001 (2017).
[13] L. Cywiński, R. M. Lutchyn, C. P. Nave, and S. Das Sarma, Phys. Rev. B **77**, 174509 (2008).
[14] C. A. Ryan, J. S. Hodges, and D. G. Cory, Phys. Rev. Lett. **105**, 200402 (2010).
[15] J. M. Cai, B. Naydenov, R. Pfeiffer, L. P. McGuinness, K. D. Jahnke, F. Jelezko, M. B. Plenio, and A. Retzker, New J. Phys. **14**, 113023 (2012).
[16] S. F. Huelga, Á. Rivas, and M. B. Plenio, Phys. Rev. Lett. **108**, 160402 (2012).
[17] M. B. Plenio and S. F. Huelga, New J. Phys. **10**, 113019 (2008).
[18] R. Vasile, S. Olivares, M. G. A. Paris, and S. Maniscalco, Phys. Rev. A **83**, 042321 (2011).
[19] R. Schmidt, A. Negretti, J. Ankerhold, T. Calarco, and J. T. Stockburger, Phys. Rev. Lett. **107**, 130404 (2011).
[20] E.-M. Laine, H.-P. Breuer, and J. Piilo, Sci. Rep. **4**, 4620 (2014).
[21] B. Bylicka, D. Chruściński, and S. Maniscalco, Sci. Rep. **4**, 5720 (2014).
[22] A. W. Chin, S. F. Huelga, and M. B. Plenio, Phys. Rev. Lett. **109**, 233601 (2012); A. Smirne, J. Kołodyński, S. F. Huelga, and R. Demkowicz-Dobrzański, Phys. Rev. Lett. **116**, 120801 (2016); J. F. Haase, A. Smirne, J. Kołodyński, R. Demkowicz-Dobrzański, and S. F. Huelga, New J. Phys. **20**, 053009 (2018).
[23] A. W. Chin, J. Prior, R. Rosenbach, F. Caycedo-Soler, S. F. Huelga, and M. B. Plenio, Nat. Phys. **9**, 113 (2013).
[24] Y. Dong, Y. Zheng, S. Li, C.-C. Li, X.-D. Chen, G.-C. Guo, and F.-W. Sun, npj Quantum Inf. **4**, 3 (2018).
[25] G. Torre and F. Illuminati, Phys. Rev. A **98**, 012124 (2018).
[26] M. M. Wolf, J. Eisert, T. S. Cubitt, and J. I. Cirac, Phys. Rev. Lett. **101**, 150402 (2008).
[27] H.-P. Breuer, E.-M. Laine, and J. Piilo, Phys. Rev. Lett. **103**, 210401 (2009).
[28] A. Rivas, S. F. Huelga, and M. B. Plenio, Phys. Rev. Lett. **105**, 050403 (2010).
[29] S. Lorenzo, F. Plastina, and M. Paternostro, Phys. Rev. A **88**, 020102(R) (2013).
[30] D. Chruściński and S. Maniscalco, Phys. Rev. Lett. **112**, 120404 (2014).
[31] G. Torre, W. Roga, and F. Illuminati, Phys. Rev. Lett. **115**, 070401 (2015).
[32] M. Wittemer, G. Clos, H.-P. Breuer, U. Warring, and T. Schaetz, Phys. Rev. A **97**, 020102 (2018).
[33] B.-H. Liu, L. Li, Y.-F. Huang, C.-F. Li, G.-C. Guo, E.-M. Laine, H.-P. Breuer, and J. Piilo, Nat. Phys. **7**, 931 (2011); J. S. Tang, C.-F. Li, Y.-L. Li, X.-B. Zou, G.-C. Guo, H.-P. Breuer, E.-M. Laine, and J. Piilo, Europhys. Lett. **97**, 10002 (2012); B.-H. Liu, D.-Y. Cao, Y.-F. Huang, C.-F. Li, G.-C. Guo, E.-M. Laine, H.-P. Breuer, and J. Piilo, Sci. Rep. **3**, 1781 (2013).

[34] S. Cialdi, D. Brivio, E. Tesio, and M. G. A. Paris, Phys. Rev. A **83**, 042308 (2011); S. Cialdi, M. A. C. Rossi, C. Benedetti, B. Vacchini, D. Tamascelli, S. Olivares, and M. G. A. Paris, Appl. Phys. Lett. **110**, 081107 (2017).
[35] A. Chiuri, C. Greganti, L. Mazzola, M. Paternostro, and P. Mataloni, Sci. Rep. **2**, 968 (2012).
[36] J. Jin, V. Giovannetti, R. Fazio, F. Sciarrino, P. Mataloni, A. Crespi, and R. Osellame, Phys. Rev. A **91**, 012122 (2015).
[37] N. B. Manson, J. P. Harrison, and M. J. Sellars, Phys. Rev. B **74**, 104303 (2006).
[38] M. W. Doherty, N. B. Manson, P. Delaney, F. Jelezko, J. Wrachtrup, and L. C. L. Hollenberg, Phys. Rep. **528**, 1 (2013).
[39] D. S. Sivia and J. Skilling, *Data Analysis—A Bayesian Tutorial* (Oxford University Press, New York, 2006).
[40] J. K. Kruschke, *Doing Bayesian Data Analysis* (Academic Press, Boston, 2015).
[41] S. Sharma, Annu. Rev. Astron. Astrophys. **55**, 213 (2017).
[42] I. Schwartz, J. Rosskopf, S. Schmitt, B. Tratzmiller, Q. Chen, L. P. McGuinness, F. Jelezko, and M. B. Plenio, arXiv:1706.07134v1.
[43] J. R. Maze, A. Dréau, V. Waselowski, H. Duarte, J.-F. Roch, and V. Jacques, New J. Phys. **14**, 103041 (2012).
[44] Y. Romach, C. Müller, T. Unden, L. J. Rogers, T. Isoda, K. M. Itoh, M. Markham, A. Stacey, J. Meijer, S. Pezzagna, B. Naydenov, L. P. McGuinness, N. Bar-Gill, and F. Jelezko, Phys. Rev. Lett. **114**, 017601 (2015).
[45] S. Felton, A. M. Edmonds, M. E. Newton, P. M. Martineau, D. Fisher, D. J. Twitchen, and J. M. Baker, Phys. Rev. B **79**, 075203 (2009).
[46] V. Jacques, P. Neumann, J. Beck, M. Markham, D. Twitchen, J. Meijer, F. Kaiser, G. Balasubramanian, F. Jelezko, and J. Wrachtrup, Phys. Rev. Lett. **102**, 057403 (2009).
[47] L. T. Hall, J. H. Cole, and L. C. L. Hollenberg, Phys. Rev. B **90**, 075201 (2014).
[48] H.-S. Zeng, N. Tang, Y.-P. Zheng, and G.-Y. Wang, Phys. Rev. A **84**, 032118 (2011).
[49] B. Vacchini, A. Smirne, E.-M. Laine, J. Piilo, and H.-P. Breuer, New J. Phys. **13**, 093004 (2011).
[50] C. Addis, B. Bylicka, D. Chruściński, and S. Maniscalco, Phys. Rev. A **90**, 052103 (2014).
[51] See Supplemental Material at http://link.aps.org/supplemental/10.1103/PhysRevLett.121.060401, which includes Refs. [52–54], for an introduction to the N-*V* center, Bayesian Inference and a detailed description of the probabilistic models employed for the FID curve and the non-Markovianity measure.
[52] M. D. Homan and A. Gelman, J. Mach. Learn. Res. **15**, 1593 (2014).
[53] R. M. Neal, Technical Report No. CRG-TR-93-1, University of Toronto (1993).
[54] J. Salvatier, T. V. Wiecki, and C. Fonnesbeck, PeerJ Comp. Sci. **2**, e55 (2016).
[55] For an incoherent mixture of the nitrogen spin, the correlation would be classical. However, the induced effect [Eq. (4)] on the reduced state of the electron spin would be the same.
[56] M. Steiner, P. Neumann, J. Beck, F. Jelezko, and J. Wrachtrup, Phys. Rev. B **81**, 035205 (2010).
[57] F. Wang, P.-Y. Hou, Y.-Y. Huang, W.-G. Zhang, X.-L. Ouyang, X. Wang, X.-Z. Huang, H.-L. Zhang, L. He, X.-Y. Chang, and L.-M. Duan, arXiv:1801.02729v1.
[58] S. Peng, X. Xu, K. Xu, P. Huang, P. Wang, X. Kong, X. Rong, F. Shi, C. Duan, and J. Du, arXiv:1801.04681v1.